Study of columnar growth, texture development and wettability of reactively sputter-deposited TiN, ZrN and HfN thin films at glancing angle incidence

Rubenson Mareus, Cédric Mastail, Firat Anğay, Noël Brunetière, Gregory Abadias

Study of columnar growth, texture development and wettability of reactively sputter-deposited TiN, ZrN and HfN thin films at glancing angle incidence

Rubenson Mareus[1,2], Cédric Mastail[1], Fırat Anğay[1], Noël Brunetière[3] and Gregory Abadias[1]

1 Institut Pprime, Département Physique et Mécanique des Matériaux, Université de Poitiers-CNRS-ENSMA, 11 Boulevard Marie et Pierre Curie, TSA 41123, 86073 Poitiers Cedex 9, France ;

2 Département Physique, Université d'Etat d'Haïti-Ecole Normale Supérieure, Laboratoire des Sciences pour l'Environnement et l'Energie (LS2E), HT6115 Canapé-Vert, Port-au-Prince, Haïti ;

3 Institut Pprime, Département Génie Mécanique et Systèmes Complexes, Université de Poitiers-CNRS-ENSMA, 11 Boulevard Marie et Pierre Curie, TSA 41123, 86073 Poitiers Cedex 9, France

Abstract: In this work, TiN, ZrN and HfN thin films fabricated using glancing angle deposition (GLAD) technique are studied both experimentally and by numerical simulations. The films (~1 μm thickness) were deposited by reactive magnetron sputtering at 0.3 Pa and 300°C on Si substrates inclined at α=85° with respect to the target. The film morphology and crystal structure were characterized by scanning electron microscopy, atomic force microscopy and X-ray diffraction (XRD), including pole figure measurements. The wettability of these coatings was investigated using the sessile drop method with three different liquids. It is shown that TiN, ZrN and HfN films have a cubic, NaCl-type crystal structure with a [111] out-of-plane orientation and exhibit a biaxial texture. XRD pole figures reveal that the crystal habit of the grains consists of {100} facets constituting triangular-base pyramids. The films develop columnar microstructures, with typical column widths of ~ 100 nm. The tilt angle β of the columns is found to increase from 24.5, 31.5 to 34° for TiN, ZrN and HfN films, respectively. Atomistic computations of the growth of these nitrides at glancing angle using a kinetic Monte Carlo model reveal that the growth morphology and variation in column tilt angle is well reproduced by considering the difference in the angular distribution of the sputtered particles. This study also shows that GLAD films are hydrophilic comparatively to the same films deposited at near-normal incidence, and among the three nitrides, TiN is the more wettable coating.

1. Introduction

Besides their traditional use as hard protective coatings, conductive transition metal nitride (TMN) thin films are also employed in key technological sectors ranging from micro- and optoelectronics [1], optics [2] and plasmonics [3–7], biomedical [8–11], as well as energy storage and conversion [12–14] due to their good electrical and optical conductivity and chemical inertness. TMN thin films and coatings are usually produced by sputter-deposition, a physical-vapor deposition technique which enables the control of the film microstructure and residual stress by appropriate tuning of the process parameters, such as working pressure, substrate temperature, ion flux energy and density. [15–18].

For some applications, it is required to produce films with enhanced surface area and porosity: e.g., in material electrodes to be integrated in supercapacitors [13,14] or in biocompatible coatings to ensure cell proliferation [10]. One can take advantage of film deposition at inclined or glancing incidence with respect to the substrate surface, known as off-normal or glancing angle deposition (GLAD) technique, to design unique film morphologies, typically consisting of inclined columns separated by intercolumnar porosity. The porosity increases with substrate inclination angle α and values ranging from 50 to 90% can be typically obtained at $\alpha = 85°$ depending on the material mobility [19,20]. The GLAD technique is in practice relatively easy to implement, as it consists in simply tilting the substrate with respect to the target. There exist variants of this technology, which imply a more sophisticated motion of the substrate, by both changing the tilt and azimuthal angles or the use of dynamic tilting during growth [19,21].

By setting the incoming particle flux at highly oblique angles with respect to the normal of the substrate, the growth mechanism is mainly governed by shadowing effects. Although numerous works have been dedicated to understand the columnar growth and texture development in off-normally deposited films [22–25], fundamental studies on TMN films

deposited at GLAD conditions are relatively scarce [26,27], although promising properties have been recently achieved [13,14,28,29]. In particular, TiN films were found to exhibit a biaxial texture [30], in which the growing crystallites possess both a specific out-of-plane and in-plane preferred orientations. While for TiN films a single in-plane orientation was observed by Mahieu *et al*. [30], a double in-plane orientation was recently reported by Abadias *et al*. for the case of HfN films [31].

Our previous works have revealed that the microstructural features of TiN and HfN GLAD films produced by magnetron sputtering are primarily dictated by the angular distribution of the particle flux [27,31]. This was achieved by varying the working pressure and substrate inclination angle α. In the present work, we extend our approach by examining the columnar growth and texture development of different materials belonging to group IVb TMN, namely TiN, ZrN and HfN, but deposited at identical GLAD conditions (α=85°). Belonging to the same column of the periodic table, Ti, Zr and Hf share the same electronic configuration (four valence electrons with a configuration of d^2s^2) and the nitride phases of these elements show similarities in their crystal structure (cubic rock-salt) and properties (high melting point, high hardness); however, being of different mass, one may anticipate a difference in the energy and angular distribution of the particles reaching the substrate due to the sputtering process and transport in the gas phase, with possible consequences on their morphology and properties that we aim to elucidate. The experimental findings are discussed and compared to 3D atomistic simulations based on a kinetic Monte Carlo (kMC) modelling of the growth process.

2. Material and Methods

2.1 Thin film preparation at GLAD conditions

TiN, ZrN and HfN thin films were deposited at 300°C on (001) Si substrates with rectangular size (2.5 cm × 1 cm) by direct current reactive magnetron sputtering. The substrate

was placed at an inclination angle α=85° with respect to the target (cathode) material to obtain GLAD conditions. The metallic Ti, Zr and Hf targets are 75 mm diameter disks with respective purity of 99.995%, 99.92% and 99.9%. They are located at 18 cm from the substrate holder in a confocal configuration, and make an angle of 25° with respect to the vertical axis of the chamber. A custom-made plate was fixed to the substrate holder to get the desired inclination angle [27,31]. The targets were operated at constant power (300 W) using a direct current power supply (Advanced Energy AE MDX 1.5K) in an Ar+N_2 plasma discharge, the gases being introduced into the chamber through separate mass flow controllers. The total working pressure (~0.3 Pa) was similar for all three material depositions, but different Ar/N_2 flow ratios were used: 16 sccm (Ar) and 0.3 sccm (N_2) for TiN, and 18 sccm (Ar) and 0.6 (N_2) for ZrN and HfN. The N_2 flow was optimized to obtain films with nitrogen content close to stoichiometry, while operating in the metallic target mode. The substrates were stationary during deposition and held at floating potentials of ~ -12, ~ 0, and ~ -9 V for TiN, ZrN and HfN films, respectively, depending on magnet configuration. Because of differences in the deposition rates between the three TMN, the deposition time was adjusted for each material to obtain GLAD films of similar thickness ($\sim$1 μm): 153, 90 and 67 min were used for TiN, ZrN and HfN films, respectively. A second set of TiN, ZrN and HfN films deposited at near-normal incidence (α=5°) were also fabricated as reference samples for wettability measurements.

2.2 Characterization methods

The morphology of the GLAD TiN, ZrN and HfN films was studied by scanning electron microscopy (SEM) using a field emission gun JEOL 7001F-TTLS microscope operating at 30 kV. The thickness and the column tilt angle β of the GLAD TiN, ZrN and HfN films were determined from cross-sectional SEM imaging. The deposition rate R was calculated from the thickness and deposition time. Plan-view SEM observations were also performed. The surface topography profile of the GLAD films was also imaged by atomic force microscopy (AFM) in

tapping mode using a Nanoscope III Multimode apparatus (Digital Instruments). The scan direction was optimized with respect to the column orientation so as to minimize tip artefact.

In order to get an estimate of the porosity, the mass density ρ of the films was derived from the position of the critical angle θ_c ($\theta_c \sim \sqrt{\rho}$), as obtained from X-ray reflectivity (XRR). XRR scans were recorded using a Seifert XRD 3000 diffractometer operated at 40 kV and 40 mA using a line focus, monochromatized Cu source, and a scintillation detector. The elemental composition of the TMN GLAD films was obtained by wavelength-dispersive X-ray spectroscopy (WDS) using an Oxford Instruments diffractometer unit attached to the JEOL microscope. Measurements were performed at 10 keV and 10 nA using Ti K_α, N K_α, Zr L_α and Hf L_α lines. Ti, Zr, AlN, SiO_2 and HfO_2 reference standards were considered for the quantitative analysis using the INCA Wave and Energy+ software, taking into account overlap correction from Ti L_α and N K_α lines.

The crystal structure of the GLAD TiN and ZrN films was examined by X-ray diffraction (XRD) using a four circle Seifert Space XRD TS-4 diffractometer operating in Bragg-Brentano θ-2θ configuration at 30 kV and 30 mA and equipped with a Meteor0D detector. XRD patterns were measured along an angular 2θ range, from 30° to 65°, using Cu K_α wavelength (1.5418 Å). This range covers the main diffraction lines of TiN, ZrN and HfN, namely 111, 200 and 220, while avoiding the main reflection from Si substrate at $2\theta = 69.13°$. We also carried out XRD pole figure measurements to analyze the texture of the GLAD films. Pole figures were acquired for {111}, {200} and {220} reflections at several sets of (ψ,ϕ) angles, where ψ is the angle between the sample surface normal and the normal to a given (hkl) plane, and ϕ is the azimuthal (polar) angle.

The room temperature electrical properties of the GLAD TiN, ZrN and HfN films were evaluated using Van der Pauw's four-point probe method [32]. The average value of electrical resistivity ρ_{el} was calculated from five measurements performed along two orthogonal in-plane

directions of the coating (longitudinal and perpendicular to the projected incoming particle flux direction).

The wettability and surface free energy (SFE) of TiN, ZrN, and HfN films deposited at α=85° (GLAD) and α=5° (reference) were determined from contact angle (CA) measurements (Krüss DSA25, Hamburg, Germany) with distilled water, diiodo-methane and ethylene glycol as wetting liquids with different polar (γ_L^p) and dispersion (γ_L^d) components, see Table 1. Contact angles θ were obtained in ambient air from the sessile drop method using a micrometric syringe and the drop image was recorded by a video camera. A volume of 2, 1 and 3 µl was used for water, diiodomethane and ethylene glycol, respectively. The mean value of the contact angle (average of left and right angles of each drop) was calculated from twenty time-dependent measurements taken at three different locations on the sample surface. The SFE of each film was calculated from the CA using the theory of Owens, Wendt, Rabel and Kaelble (OWRK) [33,34].

Table 1: Parameters of probe liquids used in evaluating SFE from CA measurements. γ_L^d and γ_L^p are the dispersive and polar component of the surface free energy: $\gamma_L = \gamma_L^d + \gamma_L^p$

Liquids	γ_L **(mJ/m²)**	γ_L^d **(mJ/m²)**	γ_L^p **(mJ/m²)**
Water	72.8	21.8	51
Diiodo-methane	50.8	50.8	0
Ethylene glycol	48	29	19

2.3 Computational approach

Atomistic computer simulations were carried out using the MODENA (Modelling Deposition of Nitride films and their Alloys) code [27,35] to simulate the growth morphology of TiN, ZrN and HfN films. This code uses a 3D rigid lattice (Na-Cl type) and is based on a kMC model to describe the deposition and diffusion events of both metallic and nitrogen species. In the present work, the angular distribution of the incoming metallic particles flux

reaching the substrate was calculated using the SIMTRA code [36]. SIMTRA simulates the transport of metallic particles from Ti, Zr or Hf target to the substrate. The angular energy distribution of the nascent particle flux (Ti, Zr and Hf sputtered atoms) leaving the target was calculated from the SRIM code [37] and used as input file for SIMTRA calculations. For the SRIM calculations, we used a threshold of 30, 40 and 61 eV for the displacement energy E_{th} of Ti, Zr and Hf, respectively, and energy of 350 eV for Ar ions [38]. These simulations give us access to a set of useful information, such as angular distribution, energy distribution, number of particles arriving at the surface of the substrate, as well as average energy of particles arriving at the surface of the substrate.

kMC simulations using the MODENA code were carried out for each material system using the corresponding SIMTRA output file obtained at a substrate inclination angle α=85°. The substrate temperature was fixed at 573 K and the same energy barriers of 1 eV for adatom diffusion were used independently of the nature of the diffusing species. An interaction parameter $r_0 = a\sqrt{2}/2$ was used for the ballistic deposition model (where a is the lattice parameter of TiN, ZrN or HfN), and the surface contact rule was defined using a minimum of 1 nearest neighbor and 3 next-nearest neighbors [35]. The size of the simulation boxes was 100 × 100× 50 a^3.

Quantitative information was obtained from the simulated growth morphology, such as the column tilt angle, the film compactness and the average layer density. The compactness is defined as the ratio between the number of particles having six nearest neighbor occupied sites to the total number of deposited particles, while the average layer density is the fraction of all occupied sites in the film plane. This latter quantity provides an estimate of the film porosity.

3. Results and discussion

3.1. Growth morphology of GLAD films

The growth morphology of cross-section GLAD TiN, ZrN and HfN films is shown in Figure 1. All films exhibit a well-defined columnar growth, with columns extending throughout the entire film thickness. As expected for GLAD geometry, the columns are oriented towards the direction of the particle flux. For the substrate inclination angle α=85°, the column tilt angle β with respect to the substrate normal is 24.5°, 31.5° and 34° for TiN, ZrN and HfN, respectively, see Table 2. The columns are straight and have a relatively constant diameter (~92, ~85 and ~110 nm for TiN, ZrN and HfN films, respectively), except in the vicinity of the substrate interface where the column density is higher.

Plan-view SEM imaging of the surface topography of the films confirms the larger size of the column ends for the HfN film, but also reveals the formation of a faceted structure (see Figure 1). The column tops emerge as triangular pyramids; however, the triangular facets are more distinctive for TiN, as also confirmed from AFM measurements (see Figure 2). It can be observed from Figures 1 and 2 that the in-plane arrangement of the columns is more regular for the TiN film: the majority of the pyramids have their side facing the projection of the particle flux (indicated by arrows). However, for the HfN film, one can notice that the columns emerge at the surface with either their side or their corner facing the incoming flux. More details about the in-plane arrangement of the columns in HfN films can be found in Ref. [31].

The root-mean-square (rms) surface roughness ω was extracted from the AFM surface profile, and the values are reported in Table 2 for the three materials. The smoothest surface is obtained for the ZrN film (ω= 50 nm). The TiN film develops a rough surface (ω= 89 nm) due to the presence of salient facets, but the roughness remains lower than that of HfN film (ω= 105 nm).

The visual inspection of the plan-view SEM images would suggest the HfN film to possess the largest porosity, in accordance with the larger inclination of the columns and larger ω value. We have estimated the porosity *P* from the mass density of the films, as derived from XRR measurements. We obtain ρ values of 1.9 ± 0.5, 2.5 ± 0.5 and 4.5 ± 1.0 g.cm^{-3} for TiN,

ZrN and HfN films, respectively. Compared to densities of bulk materials (ρ_{TiN} = 5.38 g.cm^{-3}, ρ_{ZrN} = 7.30 g.cm^{-3} and ρ_{HfN} = 13.80 g.cm^{-3}), this would correspond to a void fraction around 65 ± 10 % for all three films. Although the obtained *P* values from XRR are certainly associated with a larger uncertainty due to the significant surface roughness of the films, they are consistent with other values reported experimentally at α=85° [19,39], as well as with theoretical predictions of the porosity based on the following expression [39]

$$P_{\mathrm{th}} = 1 - \frac{R_{\alpha=0^\circ}}{R_{\alpha>0^\circ}} \cos\alpha \qquad (1)$$

where $R_{\alpha=0^\circ}$ and $R_{\alpha>0^\circ}$ are the deposition rate of the same film material grown at normal incidence (α = 0°) and oblique incidence (α > 0°), and the factor $\cos\alpha$ accounts for the geometrical reduction in the effective surface area of the substrate at inclined incidence. For α= 85°, we obtain P_{th} values of 85 ± 2 % for all three films. Note that P_{th} values calculated from Eq. (1) correspond to an upper limit of the porosity in the case of line-of-sight trajectories from the particle source, which is not the case for magnetron sputter-deposition, as it will be discussed in Sec. 3.4. Experimentally, relative densities (with respect to bulk) ranging from 10% (for low-mobility material) to 30-50% (for high-mobility metals) have been reported in the literature for α = 85° [19,40,41].

The elemental composition of the GLAD films was quantified with WDS. In addition to metal (Me) and nitrogen, the presence of oxygen in concentration ranging from 11.8 to 22.5 at.% was detected, see Table 2. For the reference films deposited at α=5° with compact microstructure, the O content was typically below 5 at.%. This suggests that oxygen atoms are primarily incorporated into the GLAD films after deposition through their porosity. For all three films, the N/Me ratio was found to be close to stoichiometry, see Table 2.

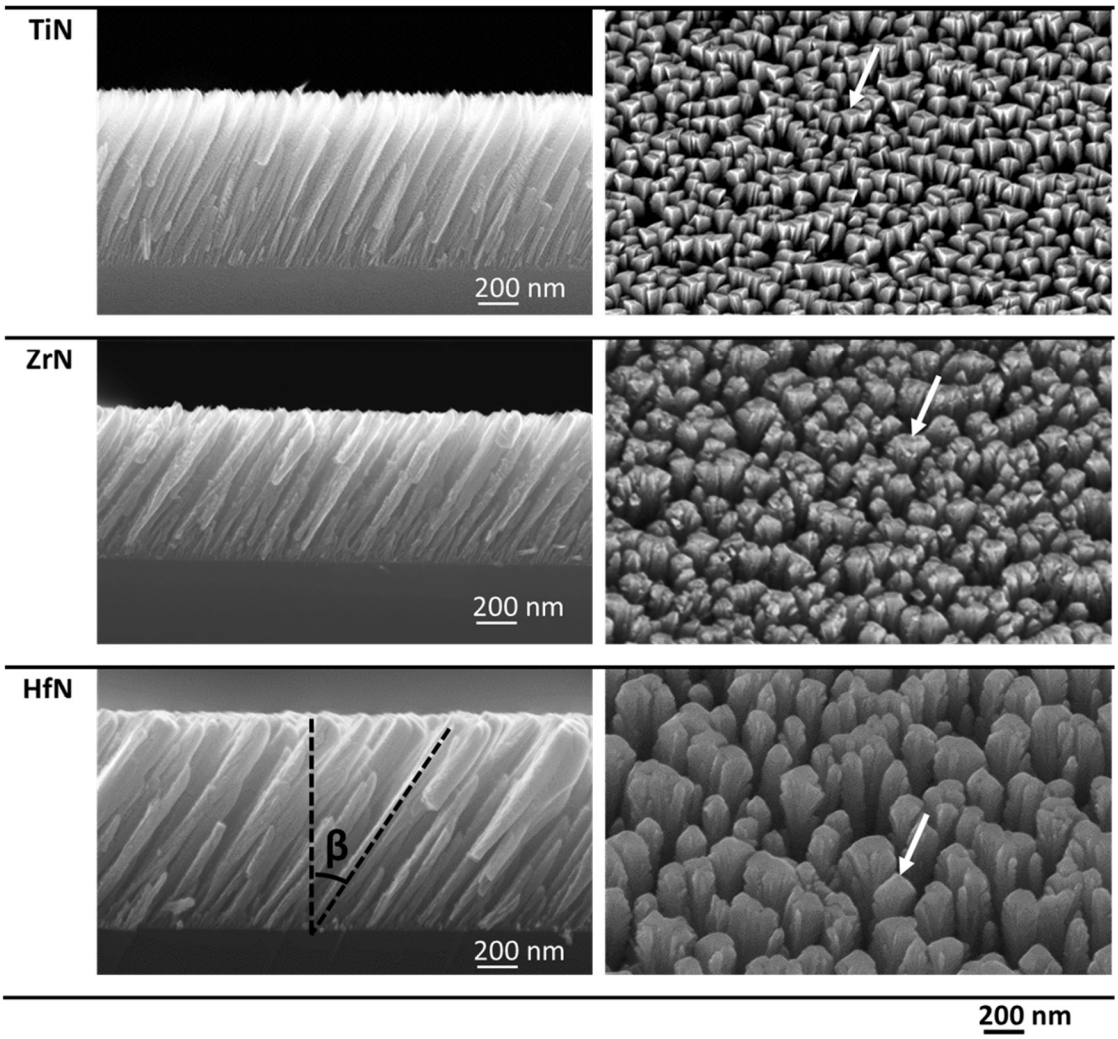

Figure 1. Cross-sectional and plan-view SEM images of TiN, ZrN and HfN films deposited at $\alpha = 85°$, 300°C and 0.3 Pa. The column tilt angle β is shown on the cross-sectional SEM image of the HfN film. The white arrows indicate the direction of the particle flux.

The electrical resistivities of the GLAD films are reported in Table 2. The measured ρ_{el} values range between 3×10^3 to 1.6×10^4 μΩ.cm, which is 2 to 3 order of magnitudes higher than that of dense, stoichiometric epitaxial TiN, ZrN and HfN layers with high crystalline quality, being 12.4 μΩ.cm [42], 12.0 μΩ.cm [43] and 14.2 μΩ.cm [44], respectively. This is mainly contributed to the presence of voids in the GLAD films. The larger resistivity of the ZrN film can be explained by a larger deviation of the N/Me ratio from stoichiometry, higher O content (22.5 at.%) and worse crystallinity.

Table 2: Structural, morphological and electrical properties of GLAD TiN, ZrN and HfN films. Also indicated is the N/Me ratio and oxygen content present in the films, as quantified by WDS.

Substrate angle α=85°	TiN	ZrN	HfN
Film thickness (nm)	900 ± 20	800 ± 20	1065 ± 20
RT resistivity ρ_{el} (μΩ.cm)	$3.0 \pm 0.5 \times 10^3$	$1.6 \pm 1.0 \times 10^4$	$9.0 \pm 2.0 \times 10^3$
Columns tilt angle β(°)	24.5 ± 2	31.5 ± 2	34.0 ± 2
Crystal tilt angle ζ(111)	3.9 ± 1	9.8 ± 1	9.0 ± 1
Surface roughness (nm)	89	50	105
N/Me ratio	1.1	1.2	0.9
O content (at.%)	12.0 ± 1.0	22.5 ± 2.0	11.8 ± 1.5

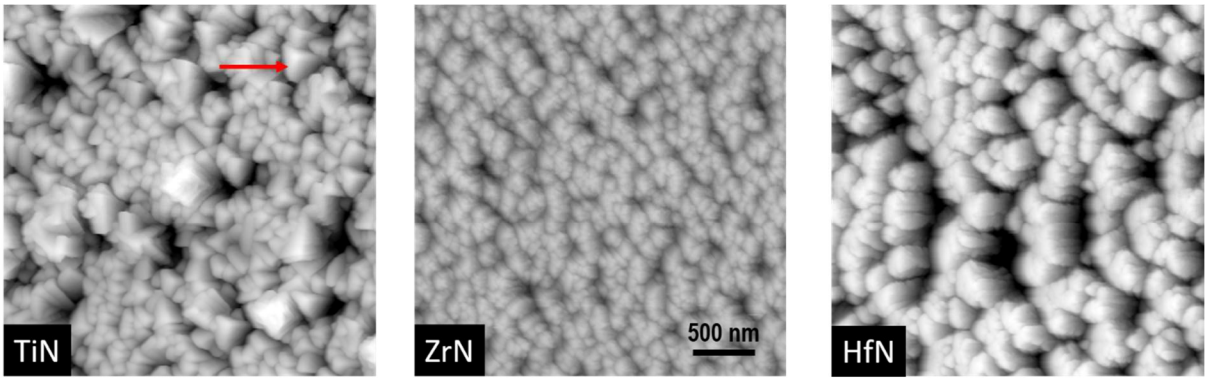

Figure 2: 3 × 3 μm^2 AFM micrographs of a) TiN, b) ZrN and c) HfN films deposited at α=85°, 300°C and 0.3 Pa. The red arrow indicates the direction of the particle flux (common for the three images).

3.2. Texture development in GLAD films

The XRD patterns of the GLAD films reported in Figure 3 show the presence of relatively sharp diffraction lines corresponding to 111, 200 and 220 Bragg reflections expected for the cubic (Na-Cl type) structure of TiN, ZrN and HfN. The most intense reflection is 111 in all cases. However, for the TiN film, it is the only line detected in the scanned 2θ range. This would suggest a stronger [111] preferred orientation for the TiN film. The issue of texture

development will be examined in more details from XRD pole figure measurements that are presented below.

For all GLAD films, the position of XRD lines corresponds to the position reported in the literature for bulk powders (see JCPDS cards N° 38-1420, 35-0753, and 33-0592 for TiN, ZrN and HfN, respectively). XRD stress analysis (not reported here) confirms that the GLAD conditions result in the development of tensile stress of low magnitude, in the 50-200 MPa range.

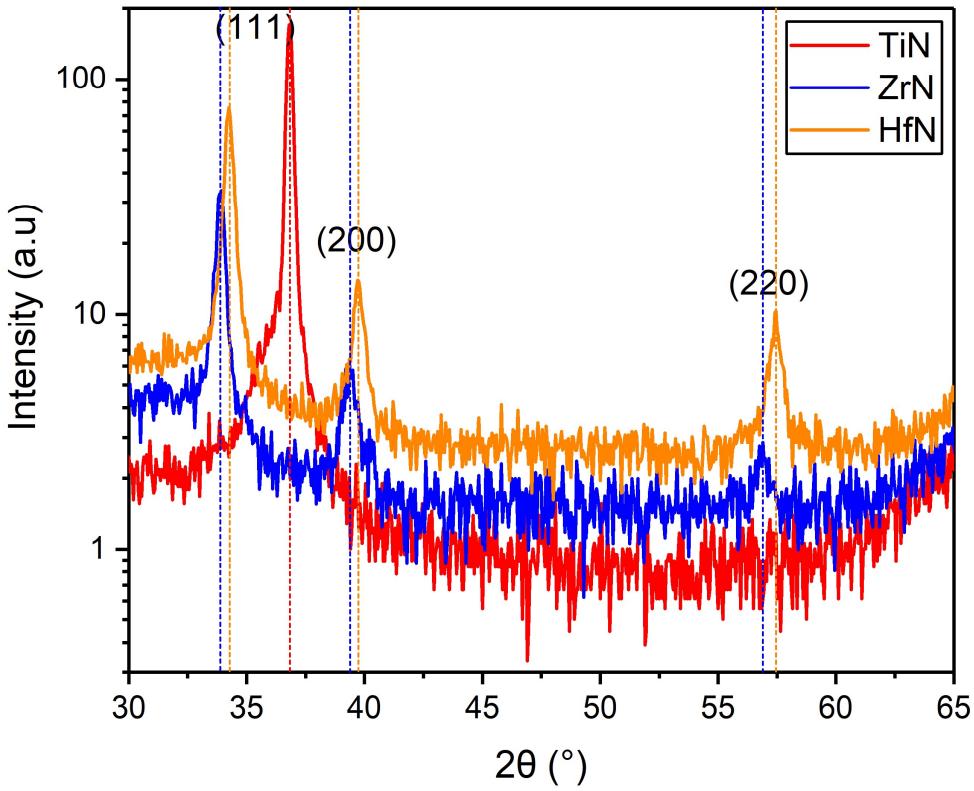

Figure 3. XRD patterns (logarithmic scale) of GLAD TiN, ZrN and HfN films at α=85° substrate inclination angle. Vertical dashed lines indicate positions for bulk reference powders.

Figure 4 displays the {111} and {200} XRD pole figures for the TiN, ZrN and HfN films deposited at α=85°. It is revealed that all GLAD films have a *biaxial* texture, i.e. they develop both out-of-plane and in-plane preferential orientations. For all samples, the highest intensity is found near the center of the {111} pole figure, confirming that films develop a (111) preferred orientation. However, as evidenced from Figure 4, the maximum is not exactly located at the

center, which means that (111) planes are slightly tilted with respect to the film surface (see values of the crystal tilt angle ζ reported in Table 2). For TiN, the {111} pole figure has one sharp maximum located at ψ=3.9° and three maxima located at ψ=72.7° for ϕ=60 and 300° and ψ=66.5° for ϕ=180°. Three intensity poles are found for the {200} reflections, located at ψ=57.8° and ϕ=0°, and ψ=52.4°for ϕ=120 and 240°. The highest {200} intensity is found along the incoming flux direction (ϕ=0°). Both pole figures evidence a threefold symmetry consistent with a (111)-oriented cubic single-crystal.

The {111} and {200} pole figures of the GLAD ZrN film exhibit similar features. However, the position of the central 111 pole is further moved away from the center, its maximum being found at ψ=9.8°. The intensity distribution of the poles located at (ψ, ϕ) = (74°, 60°), (74°, 300°) and (59°, 180°) for the {111} pole figure and (ψ, ϕ) = (64°, 0°), (46°, 120°) and (46°, 240°) for the {200} pole figure appears more spread along the ϕ direction compared to that of TiN, or even split into two maxima for the {111} pole figure (see Figure 4b). For the GLAD HfN film, the tilt of the (111) planes is 9.0°, which is similar to that of ZrN. Another striking difference is the presence of additional intensity maxima located at ϕ=0, 117 and 243° for the {111} pole figure, and at ϕ=55°, 180 and 305° for the {200} one (marked with triangles in Figure 4c), which can be consistently explained by considering a second growth variant which is in-plane rotated by 180° along the [111] axis, see Ref. [31] for more details. The location of the intensity poles is well reproduced (see square and triangle symbols in Figure 4) by considering that GLAD films develop a tilted (111) texture, with the [111] axis being tilted with respect to the surface normal by an angle ζ increasing from 3.9 for TiN to ~9-10° for ZrN and HfN. These results confirm our previous findings on the correlation between crystal tilt angle ζ and column tilt angle β [31].

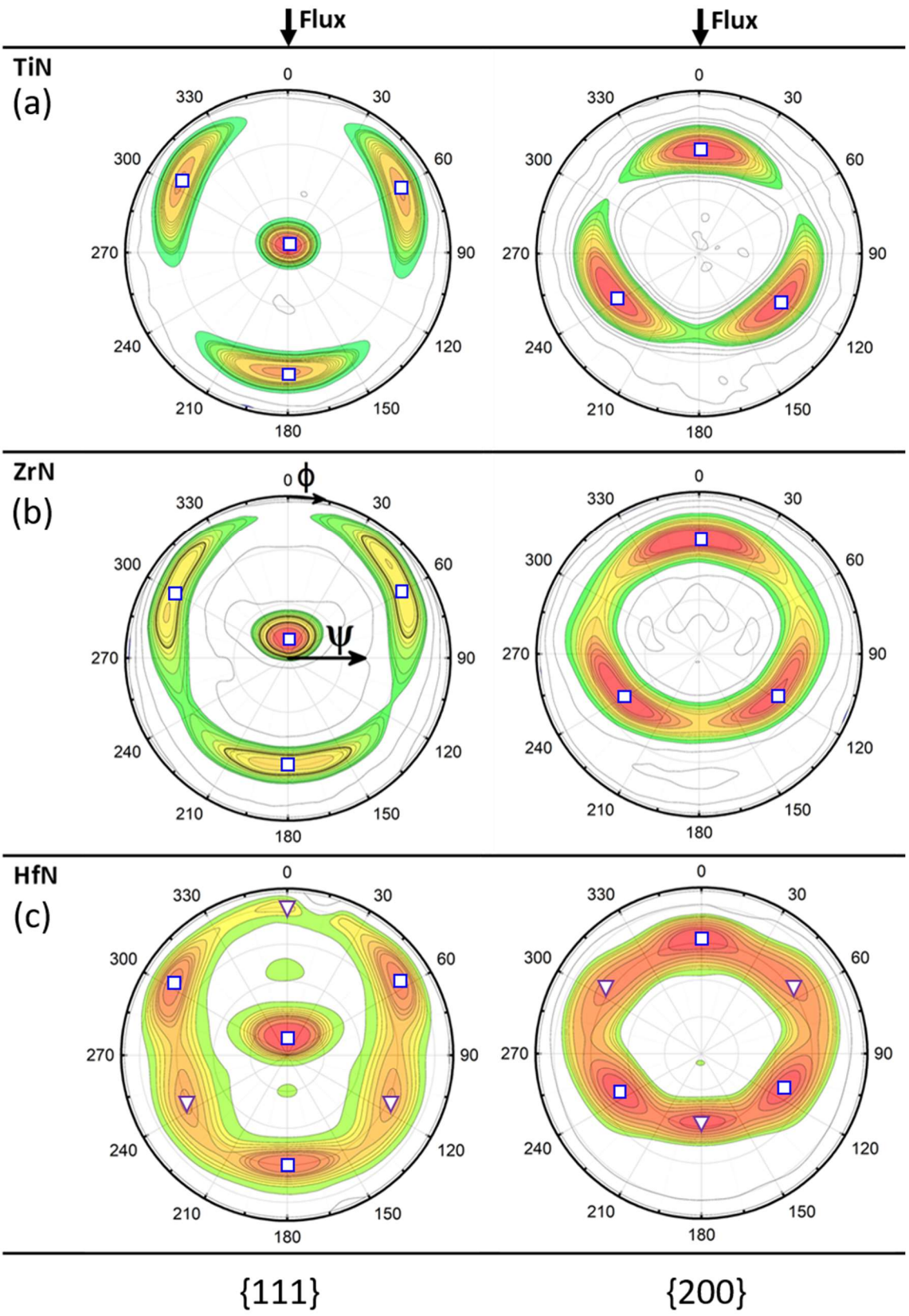

Figure 4. {111} and {200} XRD pole figures of GLAD a) TiN, b) ZrN and c) HfN films deposited at α=85° substrate inclination angle. The color scale corresponds to normalized iso-line intensity (in logarithmic scale). The incoming flux direction is aligned along ϕ=0°. Square

symbols show the theoretical pole positions. For the HfN film, a second in-plane orientation, rotated by 180° along the texture axis, is visible (marked with triangles).

The development of a biaxial texture has been already reported for off-normally deposited TMN films [26,31,45] and related to the evolutionary growth model proposed by van der Drift [46] in which grains with the geometrically fastest growing direction perpendicular to the substrate, here [111], are the ones to survive, while the in-plane alignment of the crystals is dictated by their maximum capture cross-section with respect to the incoming flux direction [26]. In the case of TiN films sputter-deposited at low N_2 pressure, Mahieu *et al*. [26] have shown that the growing crystals have a triangular-base pyramidal shape with [111] out-of-plane orientation and {100} crystal facets. SEM, AFM and XRD observations of our GLAD TiN film support this interpretation. According to Figure 1, all pyramids are oriented in such a way that their side is facing the incoming particle flux. For the GLAD HfN film, XRD pole figures of Figure 4c attest of a double in-plane alignment, which has been explained by the existence of pyramids with either their top or their side facing the incoming flux [31], in agreement with SEM observations of Figure 1.

3.3. Wettability of reference and GLAD films

Representative optical micrographs of water droplets in contact with TiN, ZrN and HfN surfaces are displayed in Figure 5 for GLAD and reference films. While reference films deposited at near normal incidence (α=5°) are hydrophobic, with typical water droplet CA of ~96°, GLAD samples turn to be hydrophilic, with CA values decreasing down to ~21°, ~17° and ~7° for HfN, ZrN and TiN films, respectively. The same trends (improved wettability for GLAD films) are observed when using the two other liquids (see Table 3).

The present results on reference films are consistent with those reported in the literature: e.g. Abdallah *et al*. [47] reported CA values of approx. 85°, 62° and 46° for stoichiometric ZrN_x (x=0.91-1.22) films in contact with water, ethylene glycol and diiodo-methane, respectively, in good agreement with our CA values of 96°, 60° and 45° found for ZrN. A similar water droplet CA value of 95° was also reported by Musil *et al*. [48] for sputter-deposited ZrN films. A slightly lower value of 75° was obtained by Chien *et al*. for TiN coatings obtained by RF sputtering [10]. The hydrophobicity character of TiN, ZrN and HfN is ascribed to the low electronegativity of group IVb transition metals [49].

The variations in CA are correlated to changes in the SFE, and generally larger CA reflects lower SFE. The SFE of the reference and GLAD films were extracted from CA measurements according to the OWRK model, and values are reported in Table 3. In this approach, the Young's equation is modified to incorporate the dispersive and polar components of the SFE, according to

$$\gamma_L(1+\cos\theta) = 2\sqrt{\gamma_S^p \gamma_L^p} + 2\sqrt{\gamma_S^d \gamma_L^d} \qquad (1)$$

where θ is the CA, γ_S^p (resp. γ_L^p) and γ_S^d (resp. γ_L^d) are the polar and dispersive part of the SFE of the TMN films (resp. probe liquid), respectively. For reference films, the SFE decreases from 44 to 38 and 33 mJ/m^2 for TiN, ZrN and HfN, respectively. These values are in line with other published values of TMN thin films and coatings: approx. 40 mJ/m^2 for TiN [8,10,50] and 35 mJ/m^2 for ZrN [8,47]. The polar component is found to be negligible for all reference TMN films. For GLAD films, an apparent and significant increase of the SFE is found compared to reference films: γ_S= 70.5 ± 1.3, 65.4 ± 3.8 and 56.1 ± 1.2 mJ/m^2 for TiN, ZrN and HfN films deposited at α=85°, respectively (see Table 3).

Based on these findings, it can be concluded that the wettability is significantly enhanced for GLAD films, and among the GLAD TMN films, TiN exhibits the stronger wetting

character. The SFE is affected by many factors, including surface chemistry and surface roughness. An increase in surface roughness will provide more contact area to the spreading liquid. The values reported in Table 3 are obtained from Eq. (1), which is only valid for a liquid sitting over a flat, smooth and chemically homogeneous surface. While for reference films this assumption may be valid because of their low surface roughness (< 10 nm), this is no longer the case for GLAD films. A more appropriate analysis, considering the nanoscale surface topography [34] would be required, which was beyond the scope of the present study. Nevertheless, the larger γ_S value of the GLAD TiN film can be understood by its relatively high surface roughness (ω= 89 nm) and the existence of well-defined facets (with typical lateral size of 100 nm) comparatively to ZrN and HfN GLAD films.

Table 3. CA and SFE of TiN, ZrN and HfN thin films deposited at a substrate inclination angle α=5 and 85°.

	Contact angle θ(°)	**TiN**	**ZrN**	**HfN**
α=5°	**Water**	96.3±0.3	96.1±1.0	96.1±0.1
	Diiodo-methane	34.0±6	44.8±0.4	42.7±3.2
	Ethylene glycol	61.6±0.9	60.2±0.1	67.8±0.3
	Surface free energy			
	γ_s(mJ/m^2)	44.2±1.4	38.1±1.2	33.2±2.8
	Contact angle θ(°)	**TiN**	**ZrN**	**HfN**
α=85°	**Water**	6.9±0.8	17.0±0.6	21.0±1.1
	Diiodo-methane	0	0	0
	Ethylene glycol	4.9±1.4	9.7±1.1	12.7±0.2
	Surface free energy			
	γ_s(mJ/m^2)	70.5±1.3	65.4±3.8	56.1±1.2

According to Lugscheider and Bobzin [50], coatings with relatively low SFE (and a low polar component) would experience a good resistance against adhesion. The present findings obtained from CA measurements on reference films deposited under conventional (near-normal incidence) conditions confirm that group IVb TMN are propitious coatings for tribological applications. Among the three studied TMN, the GLAD TiN film exhibits the larger polar

component (γ_S^p ~ 19.7 mJ/m^2), corresponding to a fractional polarity close to 0.3, a value which is thought to lead to maximum cell adhesion [51]. Therefore, the GLAD TiN film would be a suitable coating with optimum fibroblast compatibility for biomedical applications.

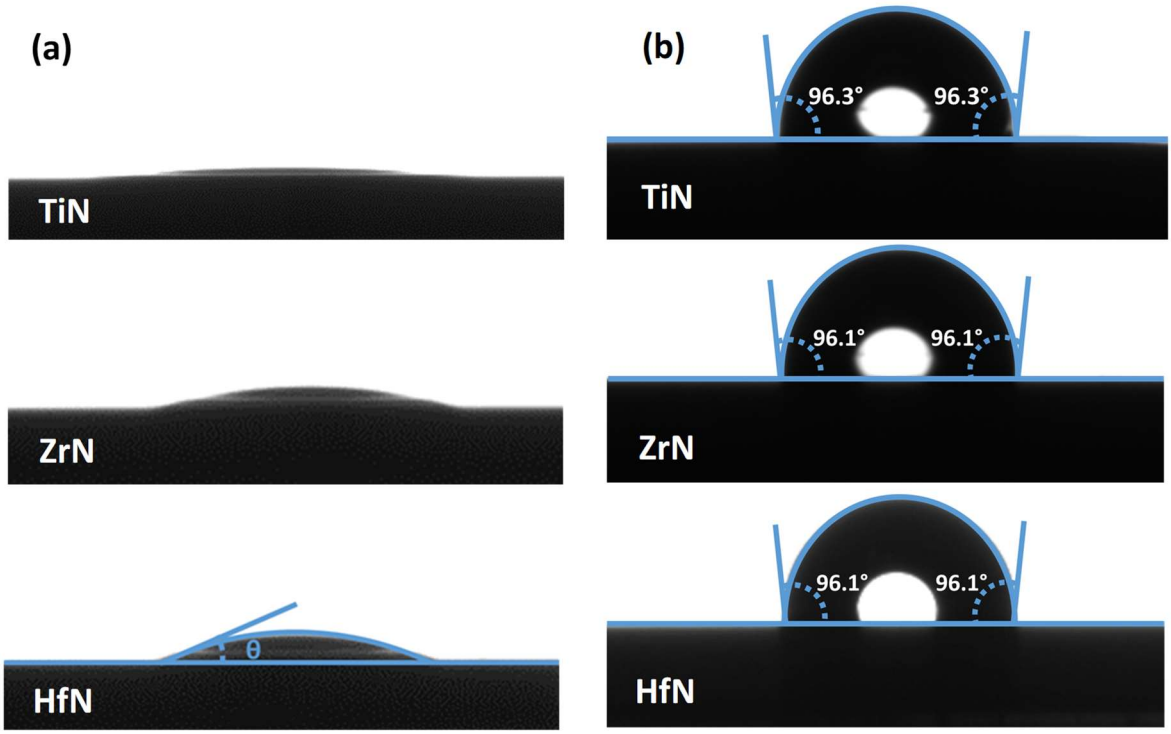

Figure 5. Water droplet CA of TiN, ZrN and HfN films (a) deposited at GLAD condition α=85° and (b) near-normal incidence α=5°. The CA θ is indicated on the HfN image at α=5°.

3.4. Prediction of growth morphology from kMC computations

The angular and energy distributions of the particle flux (sputtered atoms) leaving the target have been calculated using SRIM. The mean energy *E* of sputtered Ti, Zr and Hf atoms is 25.5, 36.7 and 30.0 eV, respectively. The variation in the energy of sputtered particles is accompanied by an increase in the sputter yield from 0.49 for Ti to 0.60 for Zr and 0.63 for Hf, primarily due to the increasing mass of the constituent metal of the target. SIMTRA calculations show that, at 0.3 Pa and α=85°, sputtered atoms experience a significant number of collisions (~20-25 in average, see Table 4) before reaching the substrate surface. As a consequence of these collisional events in the gas phase, sputtered atoms lose their kinetic energy. Because of a

similar mass with Ar gas atoms, the decrease in the average energy is most pronounced for Ti atoms, from 25.5 eV at the target position to 5.9 eV at the substrate position (see Table 4). As judged from the results plotted in Figure 6a, the energy distribution looks the same for the three elements, with a preponderant peak below 0.05 eV (corresponding to thermalized particles). However, by plotting the distribution in a logarithmic scale, one can observe a higher fraction of energetic particles for Hf (see the high energy tail over 100 eV in Figure 6b).

The angular distribution of Ti, Zr and Hf sputtered atoms reaching the substrate (positioned at α=85°) is shown in Figure 7. It can be observed that the distribution is centered at ~ 78° for Hf and Zr particles, i.e. close to the geometric inclination angle of the substrate. However, the distribution is comparatively broader for Zr, with an asymmetry towards lower angles. In contrast, the distribution of Ti particles spreads over more than 40° and is approx. centered at 50°. This reflects a larger scattering in the gas phase for Ti particles. This means that even at glancing angle (α=85°), the vast majority of Ti particles collected on the substrate surface comes from diverse directions, losing benefit of line-of-sight trajectory. Consequently, a higher number of particles arrive at the substrate (see Table 4). In a previous study [27], we have shown that the broadening of the angular distribution, and the resulting columnar morphology of GLAD TiN films, critically depended on the working pressure. Thereby this parameter is of paramount importance for GLAD technology implying sputter-deposition process.

Table 4. Results of SIMTRA calculations performed at substrate inclination angle α=85°

Substrate angle α=85°		Ti	Zr	Hf
nascent	Average energy E(eV)	25.5	36.7	30.0
0.3 Pa	Average energy E(eV)	5.2	12.3	17.7
0.3 Pa	Number of collisions	23	26	20
0.3 Pa	Number of particles reaching the substrate	27841	20025	13783

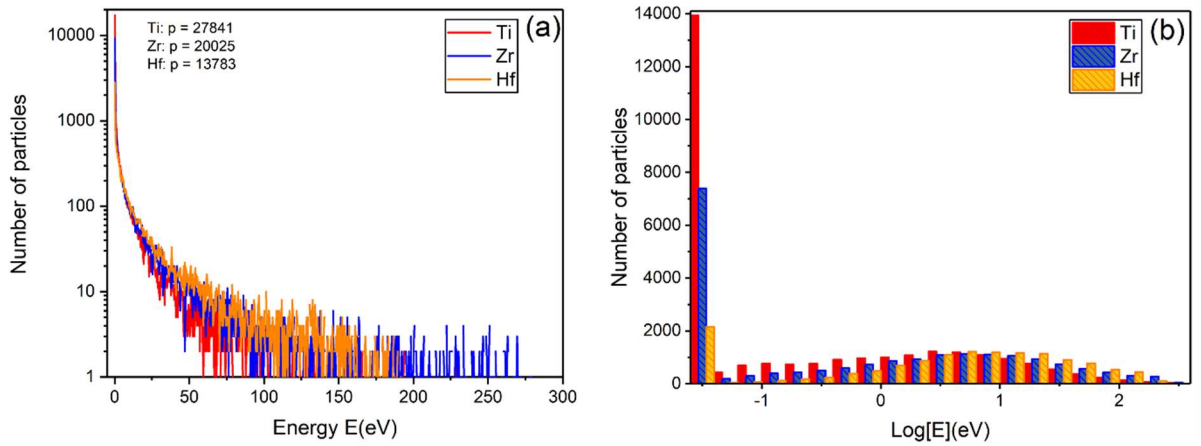

Figure 6. Energy distribution of sputtered Ti, Zr and Hf particles at the substrate position calculated using SIMTRA code for α=85° and at a fixed Ar working pressure (0.3 Pa). The number of particles p is indicated in a).

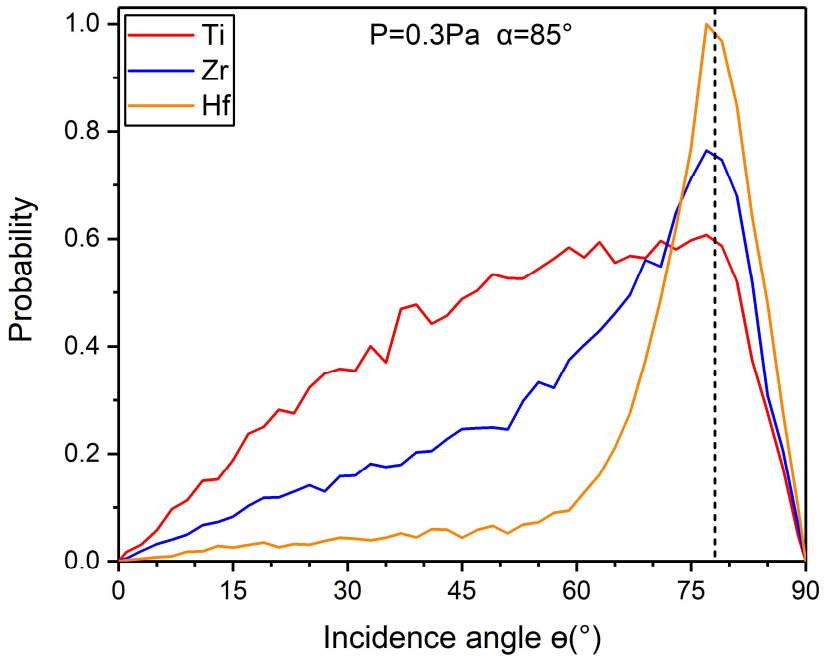

Figure 7. Angular distribution of sputtered Ti, Zr and Hf particles at the substrate position calculated using SIMTRA code at α=85° substrate inclination angle and fixed Ar working pressure (0.3 Pa). The number of particles was normalized to the highest value obtained for Hf. The total number of particles reaching the substrate is given in Table 4.

To understand the influence of the angular distribution of sputtered particles on the resulting thin film growth morphology, kMC simulations using the MODENA code were performed, with the angular distributions reported in Figure 7 as input parameters. Figure 8

shows 3D images of the simulation boxes, as well as cross-sectional views, for the TiN, ZrN and HfN films deposited at α=85°. For the sake of comparison, the angular distribution of nitrogen species was assumed to be the same as that of the metallic species, and the same diffusion barriers of 1 eV were considered for all species. The simulations adequately reproduce the experimental findings: the predicted growth morphology is composed of well-defined columns which are tilted towards the incident particle flux. The column tilt angle β increases from 40° (TiN) through 47° (ZrN) and to 54° (HfN), see Table 5. The HfN film is found to exhibit the lowest average density of 0.43 among the three TMN, which can be explained by a larger fraction of intercolumn voids (as disclosed from Figure 8) since the compactness within the columns remain essentially the same (between 0.80 and 0.88, see Table 5). The rms surface roughness increases from TiN (2 nm) to HfN (3.6 nm), in relation with the more porous morphology. Due to reduced cell dimensions compared to the experiments, absolute values of surface roughness cannot be directly compared. However, if we normalize them to the film thickness (~ 20 nm and ~ 1 μm for the computations and experiments, respectively), we obtain similar order of magnitude, ranging from 0.06-0.10 (experimentally) and 0.10-0.17 (for kMC simulations). Another striking feature of the computed morphologies is the formation of crystal facets with triangular shape, in agreement with the experiments; this is especially visible for HfN. For this latter film, the column tops have their side facing the projection of the incident flux.

From the kMC results, it can be concluded that the columnar growth of group IVb TMN films sputter-deposited at GLAD conditions is essentially governed by the angular distribution of the incident particles, and atomic shadowing effects. These findings are consistent with prior works of Siad *et al*. [52] and Bouaouina *et al*. [27]. The trend of increasing column tilt angle from TiN to HfN is qualitatively reproduced by the kMC model, although the experimental β values are smaller. This can be due to oversimplification of the used kMC model, in particular the contribution of the deposited energy (and impingement of hyperthermal particles on the

surface) is ignored, which would contribute to straighten the columns up and smooth out the surface [40]. Also, differences in energy barrier for surface diffusion are likely to explain the discrepancies between experimental and computed β values, especially at a temperature of 573 K for which such thermally-induced atomic motion processes are active.

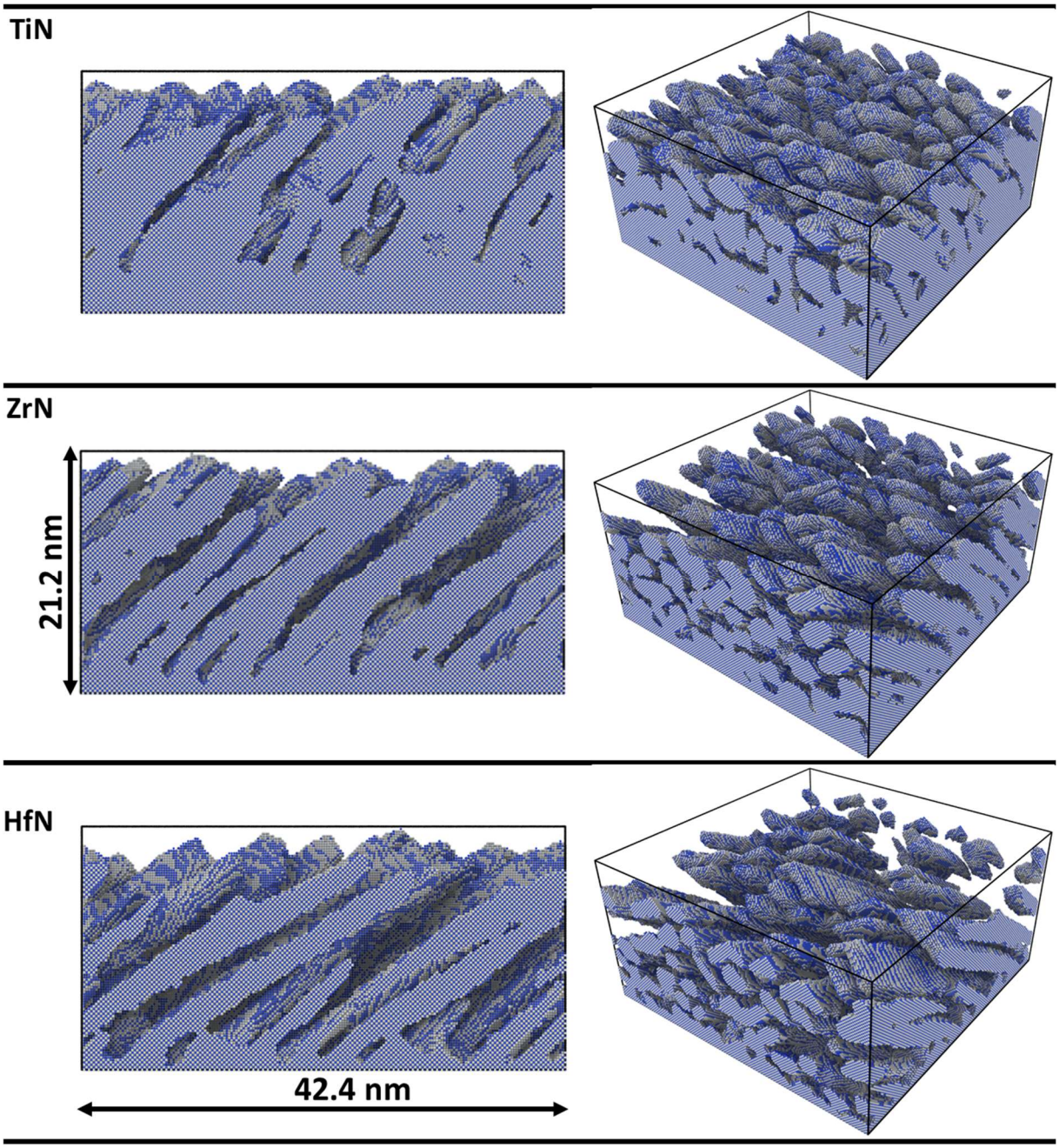

Figure 8. Cross-sectional views (in the yz plane) and 3D images of the computed TiN, ZrN and HfN growth morphology at 0.3 Pa Ar pressure and substrate inclination angle α=85°.

Table 5: Results of kMC simulations using the MODENA code for the different TMN films deposited at 573 K at substrate inclination angle α=85°.

Substrate angle α=85°		TiN	ZrN	HfN
0.3Pa	**Compactness**	0.88	0.84	0.80
	Surface roughness (nm)	2.0	2.9	3.6
	Average layer density	0.76	0.58	0.43
	Columns tilt angle β(°)	40	47	54

5. Conclusions

The present work is dedicated to the growth of TiN, ZrN and HfN films at glancing angle incidence (α=85°) by reactive magnetron sputtering. The three coatings show similar columnar growth morphology and biaxial texture development, however, a trend of increasing column tilt angle β and crystal tilt angle ξ of the basal (111) planes is evidenced with increasing mass of the transition metal. These experimental findings are qualitatively reproduced by atomistic computations based on kinetic Monte Carlo. The computations reveal that the angular distribution of the particle flux reaching the substrate is pivotal in governing the inclination of columns.

While for TiN, a single orientation is observed in the film plane, corresponding to an alignment of triangular pyramids with their side facing the projection of the particle flux, a double in-plane alignment is found for HfN. Anisotropy in surface diffusivities may likely explain these differences.

The GLAD films are found to be hydrophilic compared to the same reference films obtained at near-normal incidence. Among the group IVb TMN, TiN is found to be the more wettable coating obtained by GLAD, and would be suitable for biomedical applications.

Acknowledgments

This work partially pertains to the French Government program “Investissements d’Avenir” (LABEX INTERACTIFS, reference ANR-11-LABX-0017-01). RM acknowledges the French Ministry for Europe and Foreign Affairs for financial support through the Eiffel Excellence Scholarship Program (contract 919884J). FA acknowledges the Scientific and Technical Research Council of Turkey (TUBITAK) for fellowship granted in the frame of 2219-International Post-Doctoral Research Fellowship (contract 1059B191800197).

References

[1] I.L. Farrell, R.J. Reeves, A.R.H. Preston, B.M. Ludbrook, J.E. Downes, B.J. Ruck, S.M. Durbin, Tunable electrical and optical properties of hafnium nitride thin films, Appl. Phys. Lett. 96 (2010) 71914. doi:10.1063/1.3327329.

[2] C. Hu, K. Guo, Y. Li, Z. Gu, J. Quan, S. Zhang, W. Zheng, Optical coatings of durability based on transition metal nitrides, Thin Solid Films. 688 (2019) 137339. doi:10.1016/j.tsf.2019.05.058.

[3] U. Guler, J.C. Ndukaife, G. V. Naik, A.G.A. Nnanna, A. V. Kildishev, V.M. Shalaev, A. Boltasseva, Local heating with lithographically fabricated plasmonic titanium nitride nanoparticles, Nano Lett. 13 (2013) 6078–6083. doi:10.1021/nl4033457.

[4] P. Patsalas, N. Kalfagiannis, S. Kassavetis, G. Abadias, D.V. Bellas, C. Lekka, E. Lidorikis, Conductive nitrides: Growth principles, optical and electronic properties, and their perspectives in photonics and plasmonics, Mater. Sci. Eng. R Reports. 123 (2018) 1–55. doi:10.1016/j.mser.2017.11.001.

[5] A. Lalisse, G. Tessier, J. Plain, G. Baffou, Plasmonic efficiencies of nanoparticles made of metal nitrides (TiN, ZrN) compared with gold, Sci. Rep. 6 (2016) 38647. doi:10.1038/srep38647.

[6] Y.-J. Jen, W.-C. Wang, K.-L. Wu, M.-J. Lin, Extinction Properties of Obliquely Deposited TiN Nanorod Arrays, Coatings. 8 (2018) 465. doi:10.3390/coatings8120465.

[7] A.A. Popov, G. Tselikov, N. Dumas, C. Berard, K. Metwally, N. Jones, A. Al-Kattan, B. Larrat, D. Braguer, S. Mensah, A. Da Silva, M.A. Estève, A. V. Kabashin, Laser-synthesized TiN nanoparticles as promising plasmonic alternative for biomedical applications, Sci. Rep. 9 (2019) 1–11. doi:10.1038/s41598-018-37519-1.

[8] B. Grossner-Schreiber, M. Griepentrog, I. Haustein, W.-D. Muller, H. Briedigkeit, U.B. Gobel, K.-P. Lange, Plaque formation on surface modified dental implants. An in vitro study, Clin. Oral Implants Res. 12 (2001) 543–551. doi:10.1034/j.1600-0501.2001.120601.x.

[9] L.A. Cyster, K.G. Parker, T.L. Parker, D.M. Grant, The effect of surface chemistry and nanotopography of titanium nitride (TiN) films on primary hippocampal neurones, Biomaterials. 25 (2004) 97–107. doi:10.1016/S0142-9612(03)00480-0.

[10] C.C. Chien, K.T. Liu, J.G. Duh, K.W. Chang, K.H. Chung, Effect of nitride film coatings on cell compatibility, Dent. Mater. 24 (2008) 986–993. doi:10.1016/j.dental.2007.11.020.

[11] A.P. Serro, C. Completo, R. Colaço, F. dos Santos, C.L. da Silva, J.M.S. Cabral, H. Araújo, E. Pires, B. Saramago, A comparative study of titanium nitrides, TiN, TiNbN and TiCN, as coatings for biomedical applications, Surf. Coatings Technol. 203 (2009) 3701–3707. doi:10.1016/j.surfcoat.2009.06.010.

[12] Y. Zhong, X. Xia, F. Shi, J. Zhan, J. Tu, H.J. Fan, Transition Metal Carbides and Nitrides in Energy Storage and Conversion, Adv. Sci. 3 (2016) 1500286. doi:10.1002/advs.201500286.

[13] Z. Qi, B. Wei, J. Wang, Y. Yang, Z. Wang, Nanostructured porous CrN thin films by oblique angle magnetron sputtering for symmetric supercapacitors, J. Alloys Compd. 806 (2019) 953–959. doi:10.1016/j.jallcom.2019.07.325.

[14] E. Haye, A. Achour, A. Guerra, F. Moulaï, T. Hadjersi, R. Boukherroub, A. Panepinto, T. Brousse, J.J. Pireaux, S. Lucas, Achieving on chip micro-supercapacitors based on CrN deposited by bipolar magnetron sputtering at glancing angle, Electrochim. Acta. (2019). doi:10.1016/j.electacta.2019.134890.

[15] S. Mahieu, D. Depla, Reactive sputter deposition of TiN layers: modelling the growth by characterization of particle fluxes towards the substrate, J. Phys. D. Appl. Phys. 42 (2009) 53002. doi:10.1088/0022-3727/42/5/053002.

[16] G. Abadias, W.P. Leroy, S. Mahieu, D. Depla, Influence of particle and energy flux on stress and texture development in magnetron sputtered TiN films, J. Phys. D. Appl. Phys. 46 (2013) 55301.

[17] F. Cemin, G. Abadias, T. Minea, D. Lundin, Tuning high power impulse magnetron sputtering discharge and substrate bias conditions to reduce the intrinsic stress of TiN thin films, Thin Solid Films. 688 (2019) 137335. doi:10.1016/j.tsf.2019.05.054.

[18] G. Greczynski, J. Lu, J. Jensen, S. Bolz, W. Kölker, C. Schiffers, O. Lemmer, J.E. Greene, L. Hultman, A review of metal-ion-flux-controlled growth of metastable TiAlN by HIPIMS/DCMS co-sputtering, Surf. Coatings Technol. 257 (2014) 15–25. doi:10.1016/j.surfcoat.2014.01.055.

[19] K. Robbie, M.J. Brett, Sculptured thin films and glancing angle deposition: Growth mechanics and applications, J. Vac. Sci. Technol. A Vacuum, Surfaces, Film. 15 (1997) 1460–1465. doi:10.1116/1.580562.

[20] A. Barranco, A. Borras, A.R. Gonzalez-Elipe, A. Palmero, Perspectives on oblique angle deposition of thin films: From fundamentals to devices, Prog. Mater. Sci. 76 (2016) 59–153. doi:10.1016/j.pmatsci.2015.06.003.

[21] M.J.M. Jimenez, V.G. Antunes, L.F. Zagonel, C.A. Figueroa, D. Wisnivesky, F. Alvarez, Effect of the period of the substrate oscillation in the dynamic glancing angle deposition technique: A columnar periodic nanostructure formation, Surf. Coatings Technol. (2020). doi:10.1016/j.surfcoat.2019.125237.

[22] V. Elofsson, D. Magnfält, M. Samuelsson, K. Sarakinos, Tilt of the columnar microstructure in off-normally deposited thin films using highly ionized vapor fluxes, J. Appl. Phys. 113 (2013) 174906. doi:10.1063/1.4804066.

[23] S. Mukherjee, D. Gall, Structure zone model for extreme shadowing conditions, Thin

Solid Films. 527 (2013) 158–163. doi:10.1016/j.tsf.2012.11.007.

[24] J.M. Laforge, G.L. Ingram, M.T. Taschuk, M.J. Brett, Flux engineering to control in-plane crystal and morphological orientation, Cryst. Growth Des. 12 (2012) 3661–3667. doi:10.1021/cg300469s.

[25] M. Saraiva, D. Depla, Texture and microstructure in co-sputtered Mg-M-O (M = Mg, Al, Cr, Ti, Zr, and Y) films, J. Appl. Phys. 111 (2012) 104903. doi:10.1063/1.4718431.

[26] S. Mahieu, P. Ghekiere, D. Depla, R. De Gryse, Biaxial alignment in sputter deposited thin films, Thin Solid Films. 515 (2006) 1229–1249. doi:10.1016/j.tsf.2006.06.027.

[27] B. Bouaouina, C. Mastail, A. Besnard, R. Mareus, F. Nita, A. Michel, G. Abadias, Nanocolumnar TiN thin film growth by oblique angle sputter-deposition: Experiments vs. simulations, Mater. Des. 160 (2018) 338–349. doi:10.1016/j.matdes.2018.09.023.

[28] Z. Xie, X. Liu, W. Wang, C. Liu, Z. Li, Z. Zhang, Fabrication of TiN nanostructure as a hydrogen peroxide sensor by oblique angle deposition, Nanoscale Res. Lett. 9 (2014) 105. doi:10.1186/1556-276X-9-105.

[29] Y.J. Jen, T.L. Chan, B.H. Liao, Z.X. Li, W.C. Liu, M.Y. Cong, Tunable plasmonic resonances in TiN nanorod arrays, Coatings. 9 (2019) 863. doi:10.3390/coatings9120863.

[30] S. Mahieu, P. Ghekiere, G. De Winter, R. De Gryse, D. Depla, G. Van Tendeloo, O.I. Lebedev, Biaxially aligned titanium nitride thin films deposited by reactive unbalanced magnetron sputtering, Surf. Coatings Technol. 200 (2006) 2764–2768. doi:10.1016/J.SURFCOAT.2004.09.012.

[31] G. Abadias, F. Anğay, R. Mareus, C. Mastail, Texture and stress evolution in HfN films sputter-deposited at oblique angles, Coatings. 9 (2019) 712. doi:10.3390/coatings9110712.

[32] O. Bierwagen, R. Pomraenke, S. Eilers, W.T. Masselink, Mobility and carrier density in materials with anisotropic conductivity revealed by van der Pauw measurements, Phys. Rev. B. 70 (2004) 165307. doi:10.1103/PhysRevB.70.165307.

[33] K.-L. Law, H. Zhao, eds., Surface Wetting: Characterization, Contact Angle, and Fundamentals, 1st Ed., Springer, 2016.

[34] M.F. Ismail, B. Khorshidi, M. Sadrzadeh, New insights into the impact of nanoscale surface heterogeneity on the wettability of polymeric membranes, J. Memb. Sci. 590 (2019). doi:10.1016/j.memsci.2019.117270.

[35] F. Nita, C. Mastail, G. Abadias, Three-dimensional kinetic Monte Carlo simulations of cubic transition metal nitride thin film growth, Phys. Rev. B. 93 (2016) 64107. doi:10.1103/PhysRevB.93.064107.

[36] K. Van Aeken, S. Mahieu, D. Depla, The metal flux from a rotating cylindrical magnetron: a Monte Carlo simulation, J. Phys. D. Appl. Phys. 41 (2008) 205307.

[37] J.F. Ziegler, J.P. Biersack, U. Littmark, The Stopping and Range of Ions in Matter, Pergamon Press, New York, 1985.

[38] A.Y. Konobeyev, U. Fischer, Y.A. Korovin, S.P. Simakov, Evaluation of effective threshold displacement energies and other data required for the calculation of advanced atomic displacement cross-sections, Nucl. Energy Technol. 3 (2017) 169–175. doi:10.1016/J.NUCET.2017.08.007.

[39] S. Liedtke, C. Grüner, J.W. Gerlach, B. Rauschenbach, Comparative study of sculptured metallic thin films deposited by oblique angle deposition at different temperatures, Beilstein J. Nanotechnol. 9 (2018) 954–962. doi:10.3762/bjnano.9.89.

[40] R. Alvarez, J.M. Garcia-Martin, A. Garcia-Valenzuela, M. Macias-Montero, F.J. Ferrer, J. Santiso, V. Rico, J. Cotrino, A.R. Gonzalez-Elipe, A. Palmero, Nanostructured Ti thin films by magnetron sputtering at oblique angles, J. Phys. D. Appl. Phys. 49 (2016) 45303. doi:10.1088/0022-3727/49/4/045303.

[41] R. Alvarez, A. Garcia-Valenzuela, V. Rico, J.M. Garcia-Martin, J. Cotrino, A.R. Gonzalez-Elipe, A. Palmero, Kinetic energy-induced growth regimes of nanocolumnar Ti thin films deposited by evaporation and magnetron sputtering, Nanotechnology. 30 (2019) 475603.

[42] B.W. Karr, D.G. Cahill, I. Petrov, J.E. Greene, Effects of high-flux low-energy ion bombardment on the low-temperature growth morphology of TiN(001) epitaxial layers, Phys. Rev. B. 61 (2000) 16137.

[43] A.B. Mei, B.M. Howe, C. Zhang, M. Sardela, J.N. Eckstein, L. Hultman, A. Rockett, I. Petrov, J.E. Greene, Physical properties of epitaxial ZrN/MgO(001) layers grown by reactive magnetron sputtering, J. Vac. Sci. Technol. A Vacuum, Surfaces, Film. 31 (2013) 61516. doi:10.1116/1.4825349.

[44] H.S. Seo, T.Y. Lee, J.G. Wen, I. Petrov, J.E. Greene, D. Gall, Growth and physical properties of epitaxial HfN layers on MgO(001), J. Appl. Phys. 96 (2004) 878–884. doi:10.1063/1.1759783.

[45] A.R. Shetty, A. Karimi, Texture mechanisms and microstructure of biaxial thin films grown by oblique angle deposition, Phys. Status Solidi Basic Res. 249 (2012) 1531–1540. doi:10.1002/pssb.201248010.

[46] A. van der Drift, Evolutionary Selection, a principle governing growth orientation, Philips Res. Rep. 22 (1967) 267–288.

[47] B. Abdallah, M. Naddaf, M. A-Kharroub, Structural, mechanical, electrical and wetting properties of ZrN x films deposited by Ar/N2 vacuum arc discharge: Effect of nitrogen partial pressure, Nucl. Instruments Methods Phys. Res. Sect. B Beam Interact. with Mater. Atoms. 298 (2013) 55–60. doi:10.1016/j.nimb.2013.01.003.

[48] J. Musil, S. Zenkin, Kos, R. Čerstvý, S. Haviar, Flexible hydrophobic ZrN nitride films, Vacuum. 131 (2016) 34–38. doi:10.1016/j.vacuum.2016.05.020.

[49] S. Zenkin, Š. Kos, J. Musil, Hydrophobicity of Thin Films of Compounds of Low-Electronegativity Metals, J. Am. Ceram. Soc. 97 (2014) 2713–2717.

[50] E. Lugscheider, K. Bobzin, The influence on surface free energy of PVD-coatings, Surf. Coatings Technol. (2001). doi:10.1016/S0257-8972(01)01315-9.

[51] N.J. Hallab, K.J. Bundy, K. O'Connor, R. Clark, R.L. Moses, Cell adhesion to biomaterials: correlations between surface charge, surface roughness, adsorbed protein, and cell morphology, J. Long. Term. Eff. Med. Implants. 5 (1995) 209–231.

[52] A. Siad, A. Besnard, C. Nouveau, P. Jacquet, Critical angles in DC magnetron glad thin films, Vacuum. 131 (2016) 305–311. doi:10.1016/j.vacuum.2016.07.012.